AJNR

Identification of Intraplaque Hemorrhage on MR Angiography Images: A Comparison of Contrast-Enhanced Mask and Time-of-Flight Techniques

Y. Qiao, M. Etesami, S. Malhotra, B.C. Astor, R. Virmani, F.D. Kolodgie, H.H. Trout III and B.A. Wasserman

Y. Qiao
M. Etesami
S. Malhotra
B.C. Astor
R. Virmani
F.D. Kolodgie
H.H. Trout III
B.A. Wasserman

Identification of Intraplaque Hemorrhage on MR Angiography Images: A Comparison of Contrast-Enhanced Mask and Time-of-Flight Techniques

BACKGROUND AND PURPOSE: MRA is widely used to measure carotid narrowing. Standard CE- and TOF-MRA techniques use highly T1-weighted gradient-echo sequences that can detect T1 short blood products, so they have the potential to identify IPH, an indicator of plaque rupture. We sought to determine the accuracy and reliability of these MRA sequences to detect IPH.

MATERIALS AND METHODS: 3D TOF and CE carotid MRA scans were obtained at 3T on 15 patients (age range, 58–86 years; 13 men) scheduled for CEA. The source images from the precontrast (mask) CE-MRA and the TOF sequences were reviewed by 2 independent readers for IPH presence (identified as hyperintense signal intensity compared with adjacent muscle). CEA specimens were stained with antibody against glycophorin A and Mallory stain to detect IPH and were correlated with MR images.

RESULTS: Nine of 15 CEA specimens (61 of 144 MR images) contained IPH confirmed by histology. Compared with TOF, CE-MRA mask demonstrated greater sensitivity, specificity, PPV, and NPV for IPH detection. The accuracy for correctly identifying IPH by using CE-MRA mask images and TOF images was 94% and 84%, respectively. Inter- and intraobserver agreement for IPH detection was excellent by mask images ($\kappa = 0.91$ and $\kappa = 0.94$, respectively) and TOF images ($\kappa = 0.77$ and $\kappa = 0.84$, respectively).

CONCLUSIONS: CE-MRA mask images are highly accurate and reliable for identifying IPH, more so than the TOF sequence, and can potentially provide valuable information about risk for rupture.

ABBREVIATIONS: CE = contrast-enhanced; CEA = carotid endarterectomy; CI = confidence interval; CNR = contrast-to-noise ratio; ECA = external carotid artery; FFE = fast-field echo; ICA = internal carotid artery; IPH = intraplaque hemorrhage; MIP = maximum intensity projection; MPRAGE = magnetization-prepared rapid acquisition of gradient echo; MRA = MR angiography; MRDTI = MR direct thrombus imaging; NPV = negative predictive value; PPV= positive predictive value; SI = signal intensity; SPGR = spoiled gradient-recalled; T1WI = T1-weighted imaging; TOF = time-of-flight; TSE = turbo spin-echo

Noninvasive MRA has become a standard approach to assessing carotid stenosis severity, by using either CE or TOF techniques.[1] The North American Symptomatic Carotid Endarterectomy Trial and the European Carotid Surgery Trial established the benefit of identifying and treating carotid stenosis to prevent ischemic stroke.[2,3] More recent studies have used MR imaging to assess plaque components rather than the degree of narrowing and have identified features that indicate stroke risk. In particular, IPH not only indicates the risk for prior plaque rupture[4,5] but also for future embolic events.[6-9]

IPH may be difficult to distinguish from the lipid core by signal intensity on conventional T1-weighted and T2-weighted spin-echo sequences[10,11]; however, the accuracy of MR imaging for detecting IPH is improved when TOF is added to this multicontrast approach.[12] Moody et al[13] used a T1-weighted gradient-echo sequence termed "MRDTI" to detect methemoglobin-rich hemorrhage within plaque and demonstrated a strong agreement between MRDTI-detected IPH and histology. However, most radiologists do not acquire additional sequences beyond those used to measure stenosis, partly because of time constraints and a lack of familiarity with the technique and its interpretation.

CE-MRA and TOF sequences are part of the standard carotid MRA evaluation and use T1-weighted SPGR techniques, giving them the potential to detect IPH.[14] Tissues with short T1 relaxation such as fat and blood products (specifically, methemoglobin) can be identified as regions of high signal intensity on TOF-MRA images, including both source images and reconstructed MIP images.[15] Identification of IPH on a CE-MRA study can be more complicated because the MIP images are generated by subtracting the precontrast (ie, mask) from postcontrast series. Therefore, high-signal-intensity areas corresponding to blood products are removed from the MIP images, and their identification relies on evaluating the mask images.

Recent advances in high-field imaging have improved the

ability to detect carotid stenosis, with many radiologists now implementing MRA at 3T for this purpose[16]; however, an improved detectability of IPH at higher fields cannot be assumed because the paramagnetic properties of IPH can compromise its hyperintense signal intensity on T1WI from increased susceptibility at higher fields.[17] Wintermark et al[18] showed the usefulness of standard CE-MRA for the detection of bright signal intensity thought to represent IPH in 3 cases, though their results were not corroborated by histology.

In the present study, we sought to determine the reliability and accuracy of IPH detection by TOF and CE-MRA mask images, acquired as part of a standard evaluation at 3T for carotid stenosis.

Materials and Methods

Subjects

Fifteen consecutive participants underwent a 3T MR imaging examination that included CE- and TOF-MRAs for carotid artery stenosis and a subsequent CEA (13 men; mean age, 72 years; range, 58–86 years). Stenosis ranged from 58% to 99% (mean, 77%) for symptomatic ($n = 8$) and from 65% to 90% (mean, 75%) for asymptomatic patients ($n = 7$). The mean time between MR imaging and CEA was 24.4 ± 19.4 days. Institutional review board approval was obtained, and each participant provided informed consent.

MR Imaging Examination

All examinations were performed on a 3T MR imaging scanner (Achieva; Philips Healthcare, Best, the Netherlands) by using either a 4-channel (Pathway MR Imaging, Redmond, Washington) or an 8-channel[19] phased-array carotid coil. For the CE-MRA series, a 3D FFE sequence was acquired before (ie, mask) and after the intravenous injection of gadopentetate dimeglumine (0.1 mmol/kg, Magnevist; Schering, Berlin, Germany) or gadodiamide (Omniscan; GE Healthcare, Piscataway, New Jersey) in the coronal plane with the following parameters: TR/TE/flip angle, 6.0 ms/2.0 ms/30°; bandwidth, 434 Hz/pixel; matrix, 392 × 392; FOV, 260 × 260 mm²; 40 sections. The acquired voxel size was $0.66 \times 0.66 \times 1$ mm³ and was reconstructed to a matrix of 512 × 512 with interpolation to 80 sections at 0.5 mm. k-space was acquired by using an elliptic centric view ordering, and the scanning time was 1 minute 6 seconds per acquisition.

The 3D TOF-MRA was acquired by using a multiple overlapping thin-slab acquisition in the axial plane by using a 3D FFE sequence with the following parameters: TR/TE/flip angle, 23 ms/3.5 ms/25°; bandwidth, 192 Hz/pixel; matrix, 304 × 200; FOV, 160 × 160 mm²; 50 sections. The acquired voxel size was $0.53 \times 0.80 \times 1.4$ mm³ and was reconstructed to a matrix of 512 × 512 with interpolation to 100 sections at 0.7 mm. The total coverage was 70 mm, and the scanning time was 5 minutes 34 seconds.

MR Imaging Postprocessing

MR images were processed by using VesselMASS software (Division of Image Processing, Leiden University Medical Center, the Netherlands). Sections were reconstructed at 2-mm thickness for each participant from 3D CE-MRA and TOF source images at an orientation orthogonal to the long axis of the carotid artery to include the bifurcation by using the multiplanar reconstruction tool in VesselMASS.

Histology

All endarterectomy specimens were fixed in 10% formalin immediately after surgery and transferred to CVPath Institute (International Registry of Pathology, Gaithersburg, Maryland) for histologic analysis under the supervision of a cardiovascular pathologist (R.V.). Specimens were decalcified in 10% ethylenediaminetetra-acetic acid solution (pH 7.4) for 72 hours and embedded in paraffin.[20] MIP images that best profiled the luminal contour and narrowing were selected, and traversing lines were drawn (Fig 1A) that corresponded to the reformatted MR imaging section positions (Figs 1B, -C). These processed MIP images were used to orient transverse histologic sections, 5 μm thick, through the specimen (Fig 1D). The sections were stained with hematoxylin-eosin and Movat pentachrome. Glycophorin A and iron were identified by using immunochemistry and Mallory stain, respectively.

Image Analysis

An observer (Y.Q.) not involved in reading images coregistered the reformatted MR imaging sections with histology by using distances relative to the carotid bifurcation and internal plaque landmarks clearly visible by MR imaging and histology, including morphology and size of the lumen and morphology of large calcified regions. Although specimens were decalcified, areas of calcification could be identified on the basis of residual blue staining by hematoxylin-eosin. IPH was identified as hyperintense signal intensity on reformatted CE-MRA mask and TOF images compared with adjacent muscle; other plaque components, such as lipids and calcification, were iso- or hypointense, respectively.[12,13,21] Mask images were used to discriminate hyperintense signal intensity due to IPH from that attributed to luminal enhancement (Fig 2). All reconstructed images were de-identified and interpreted individually in random order by 2 independent readers (M.E. and S.M.), who were blinded to the histology results. The presence of IPH was documented for each MR image. The analysis of the TOF and CE-MRA images from the same examination was separated in time to avoid recall bias. The pathologist (R.V.) was blinded to the MR imaging results and reviewed the corresponding histology slides to document IPH presence.[13,21] IPH was considered present when its size exceeded 1.0 mm².

Regions of IPH identified by histology were used to evaluate IPH detection by MR imaging (Fig 3). Normalized CNR values of IPH relative to adjacent muscle were calculated for the 2 MRA techniques by using $\text{CNR} = (\text{SI}_{\text{IPH}} - \text{SI}_{\text{muscle}}) / \text{SD}_{\text{noise}}$, where SI_{IPH} is the signal intensity of IPH, $\text{SI}_{\text{muscle}}$ is the signal intensity of the adjacent muscle, and SD_{noise} is the SD of the signal intensity of background noise.[22]

Statistical Analysis

All analyses were performed by using the Statistical Package for the Social Sciences, Version 17.0 (SPSS, Chicago, Illinois). A random-effects model was used to account for the correlation of repeated measures within a patient and to compare CNR differences between the 2 MRA sequences. Interobserver variability was measured by using a Cohen κ statistic. A κ value of <0.4 was characterized as poor agreement; 0.4–0.75, as fair to good; and >0.75, as excellent.[23] Intraobserver variability was estimated on the basis of repeated readings (M.E.) of all MR imaging examinations after a 3-month interval to avoid recall bias. The sensitivity, specificity, PPV, and NPV, and diagnostic accuracy of plaque characteristics were calculated.
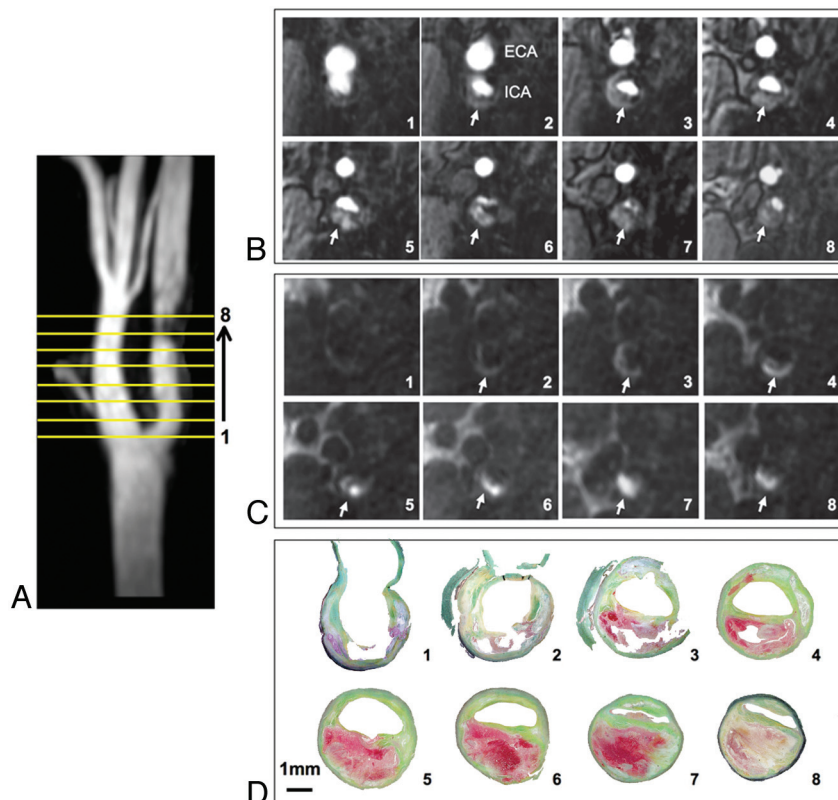
Fig 1. Coregistration of MRA and histologic images. MIP image from the TOF-MRA that profiles the narrowed lumen contour (*A*) used to show the position of 8 reformatted TOF (*B*) and CE-MRA mask (*C*) sections (reconstructed thickness, 2 mm), to orient transverse 5-μm histologic sections through the specimen (*D*). IPH is identified as hyperintense signal intensity compared with adjacent muscle on MRA images (*arrows*, *B* and *C*) and is red on histologic sections (*D*) stained with Movat pentachrome.
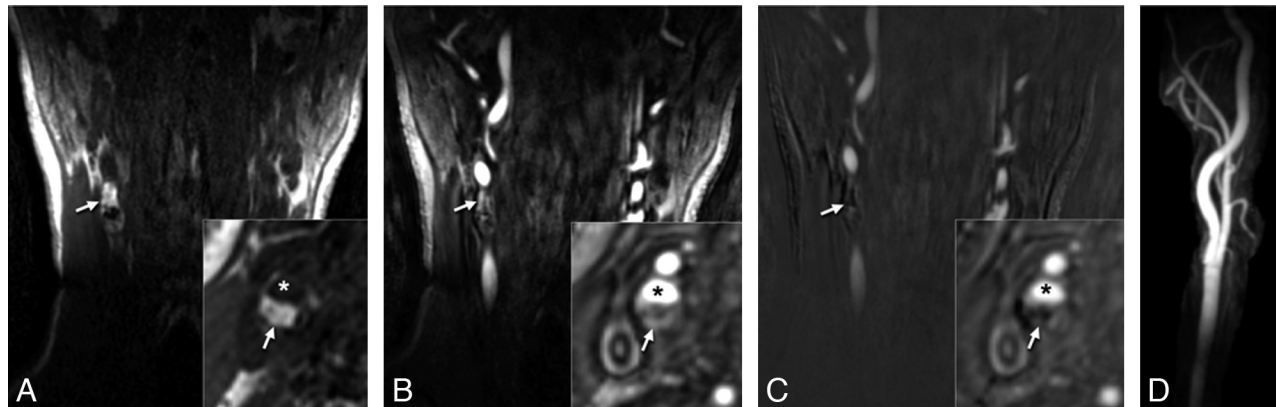

Fig 2. Identifying IPH on CE-MRA mask images in a 72-year-old man with a right cerebral ischemic event. Coronal and reconstructed axial (inset) sections from the mask (*A*) series show hyperintense signal intensity (*arrows*) in the right carotid artery wall. The high signal intensity (*arrows*) is again seen on the corresponding postcontrast images (*B*) but is removed after the mask images are subtracted from this series (*C*). (*Asterisk* indicates the lumen.) MIP images are generated from the subtracted series (*D*), so IPH information is lost.

Results

Nine of 15 patients had IPH by histology. A total of 144 reconstructed axial MR images could be matched with histology (approximately 10 MR images per patient), and 63 had IPH by histology. Compared with TOF, CE-MRA mask demonstrated higher diagnostic values, including sensitivity, specificity, PPV, and NPV for IPH detection by 2 independent readers (Table).

On the basis of the mask sequence, readers 1 and 2 accurately identified IPH on 57 (90.5%) and 53 (84.1%) images, respectively (Table). There were a total of 10 false-negative and 2 false-positive results by 2 readers. False-negative results

were due to the presence of calcification or hemosiderin or a lack of methemoglobin (Fig 4). False-positive results could be attributed to signal intensity from adjacent fat. The mean sensitivity, specificity, PPV, NPV, and diagnostic accuracy for the detection of IPH were 87%, 99%, 98%, 91%, and 94%, respectively. Intra- and interobserver agreements for IPH detection were excellent ($\kappa = 0.94$; 95% CI, 0.87–1; and $\kappa = 0.91$, 95% CI, 0.84–0.98, respectively).

On the basis of the TOF source images, readers 1 and 2 each accurately identified IPH on 50 (79.3%) images. There were a total of 17 false-negative and 14 false-positive results by 2 readers. False-negative results were also due to calcifi-
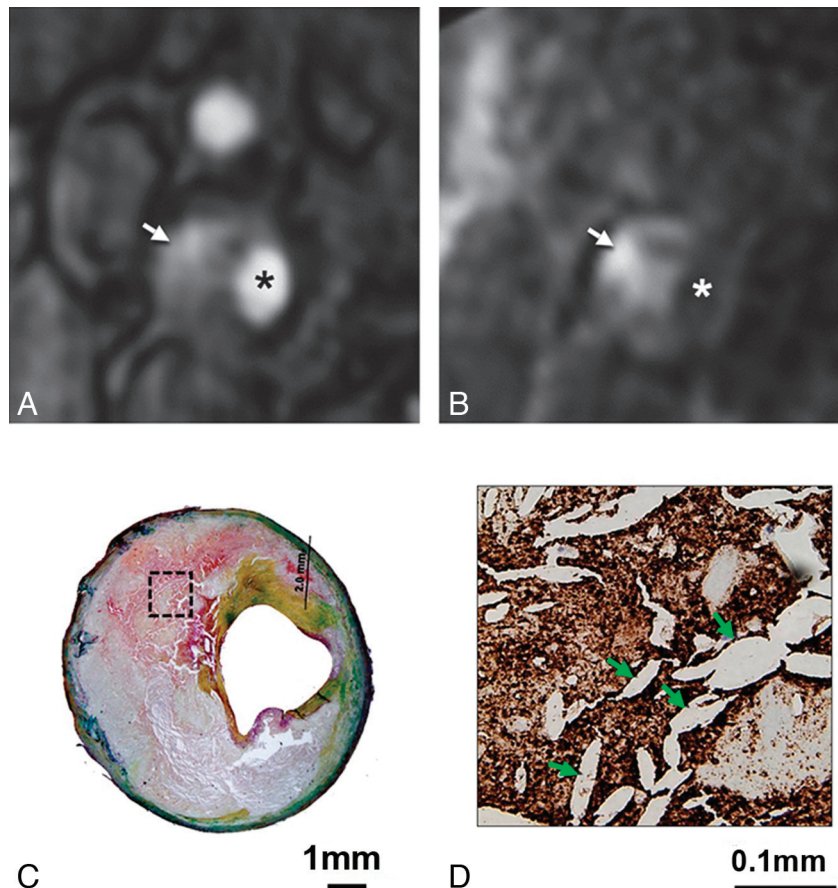
Fig 3. MRA images with matched histology for a 73-year-old man with a right cerebral ischemic event. Hyperintense signal intensity on the postcontrast (*arrow*, *A*) and mask (*arrow*, *B*) CE-MRA images (*asterisk* indicates the lumen) corresponds to red staining representing IPH on histology (*C*, Movat pentachrome stain). Immunostaining for glycophorin A (*D*) confirms the presence of erythrocytes (dark brown staining) mixed with cholesterol clefts (*arrows*, *D*) for a region within the core (*box*, *C*).

Agreement between IPH detected by MR imaging and histology

	Reader		Histology +	Histology −	Total
No. of Images			63	81	144
CE-MRA mask[a]	1	+	57	2	59
		−	6	79	85
	2	+	53	0	53
		−	10	81	91
TOF[b]	1	+	50	11	61
		−	13	70	83
	2	+	50	10	60
		−	13	71	84

[a] Reader 1: Sensitivity, specificity, PPV, and NPV (95% CI) are 90% (80%–96%), 98% (91%–100%), 97% (87%–99%), and 93% (85%–97%), respectively. Reader 2: Sensitivity, specificity, PPV, and NPV (95% CI) are 84% (72%–92%), 100% (94%–100%), 100% (92%–100%), and 89% (80%–94%), respectively.
[b] Reader 1: Sensitivity, specificity, PPV, and NPV (95% CI) are 79% (66%–88%), 86% (77%–93%), 82% (70%–90%), and 84% (74%–91%), respectively. Reader 2: Sensitivity, specificity, PPV, and NPV (95% CI) are 79% (67%–88%), 88% (78%–94%), 83% (71%–91%), and 85% (75%–91%), respectively.

cation or hemosiderin or a lack of methemoglobin. False-positive results were due to small ulcers and motion artifacts. The mean sensitivity, specificity, PPV, NPV, and diagnostic accuracy for the detection of IPH was 79%, 87%, 83%, 84%, and 84%, respectively. Intra- and interobserver agreements for IPH detection were excellent ($\kappa = 0.84$; 95% CI, 0.73–0.95; and $\kappa = 0.77$; 95% CI, 0.67–0.88, respectively).

Average CNR of IPH based on the mask image was 3.13 (95% CI, 2.17–5.15) times higher than that based on the corresponding TOF image.

Discussion

We demonstrated that IPH, an important indicator of risk for future clinical events,[6-9] can be reliably and accurately identified on source images from standard MRA sequences acquired at 3T, especially by using a CE-MRA technique. MRA is widely used to evaluate the severity of carotid luminal narrowing, and we have shown that it also provides information about IPH without additional imaging or dedicated sequences. Clinically relevant information can be disregarded if the interpreting radiologist does not know to look for it. Our results highlight the importance of MRA source images because this information is not readily identifiable on MIP images, which are often the only images reviewed when evaluating stenosis.

Detection of IPH on high-resolution carotid MR imaging has been previously reported at 1.5T by using T1-weighted techniques such as black-blood spin-echo,[4] gradient-echo,[13,21,24] and TOF[12,15] imaging. Moody et al[13] reported 84% sensitivity and 84% specificity for identifying complicated plaques (presumptive IPH) by using the MRDTI technique. Our use of the mask sequence for IPH detection at 3T revealed similar sensitivity and higher specificity estimates compared with the studies reported at 1.5T by using dedicated sequences for IPH detection. Bitar et al[21] used a
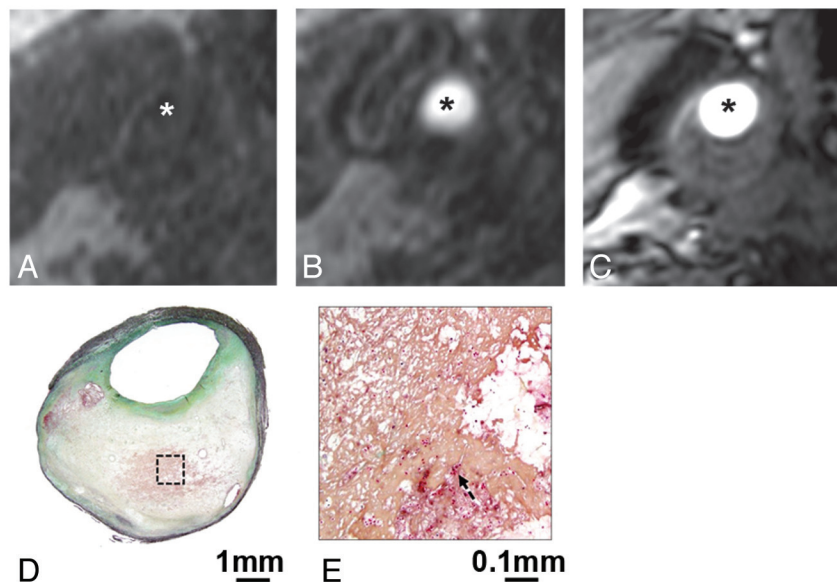
Fig 4. An example of IPH missed on both CE- and TOF-MRA. Reconstructed axial mask (*A*), postcontrast (*B*), and TOF-MRA (*C*) images in matched locations transversely through a carotid plaque show no hyperintense signal intensity to suggest IPH (*asterisk* indicates the lumen). The corresponding CEA specimen section stained with Movat pentachrome demonstrates an attenuated fibrin network. A high-power view (*E*) of a region of necrotic core (*box, D*) shows scattered erythrocytes (*arrow, E*).

high-resolution fat-suppressed T1-weighted SPGR sequence at 1.5T to identify IPH in patients scheduled for CEA and reported a slightly higher sensitivity (94%–100%) and lower specificity (80%–88%) compared with our results. However, these patients were first screened by MRDTI to select those suspected of having IPH, and this screening may have skewed the distribution of hemorrhage in this population and affected their estimates.

Only 1 other study reported IPH detection by MR imaging at 3T.[25] Ota et al[25] used a modified MPRAGE sequence similar to MRDTI and observed a higher sensitivity (80%) and specificity (97%) compared with TSE and TOF sequences based on histologic correlation, though they excluded cases with small IPH or heavy calcification that might interfere with IPH detection. Although our sensitivity was higher and specificity comparable by using a standard mask sequence, the difference could be attributed to the distribution or stage of hemorrhage within the samples. The MPRAGE sequence takes approximately 3–4 minutes to acquire. On the basis of our results and those of Ota et al, it seems that MR imaging at 3T may improve our ability to confirm IPH presence more than was previously achievable at 1.5T; this result is fortuitous, given the trend toward higher field imaging to measure carotid narrowing in routine practice.

Ulceration proved to be a frequent reason for false-positive identification of IPH on TOF images because the signal intensity of flowing blood within an ulcer is similar to that of IPH. Because the signal intensity of flowing blood is not enhanced on mask images, ulceration can be easily distinguished from IPH on this sequence, which is why mask images yielded far fewer false-positive results than corresponding TOF images for IPH detection. Mask images also resulted in fewer false-negatives because of the inherently greater CNR of IPH on these images compared with corresponding TOF images, likely because of the heavier T1-weighting achieved by the CE-MRA sequence. In addition, the TOF sequence was more

prone to motion artifacts because of the longer acquisition time needed, which contributed to false-positive IPH detection.

The superior soft-tissue contrast offered by MR imaging compared with that offered by other imaging modalities can be extended to the in vivo detection of IPH. Sonography cannot discriminate IPH from the lipid core,[26] and CT angiography is of limited utility because of the overlap of the distribution of densities between IPH and other plaque components.[27]

Limitations to our study include the following: 1) IPH signal intensity on T1WI may change as hematoma evolves from methemoglobin (hyperintense) to hemosiderin (hypointense),[4] which could limit the utility of hyperintense signal intensity as a reliable feature for IPH detection. However, we and others[5] have observed that hemorrhage in carotid plaque, unlike in the brain, may remain hyperintense for as long as 18 months, possibly because of the complex underlying core composition retarding its evolution. Furthermore, our high NPV indicates that relying on hyperintense signal intensity for IPH detection is reasonable. 2) False-negative results on both mask and TOF images can occur when blood is not present as methemoglobin, as described above, or when there is mixing of methemoglobin with tissues prone to susceptibility effects (eg, calcification or hemosiderin), as we observed in our study. This is a universal problem that would affect any of the other MR imaging sequences designed to detect IPH as well (eg, gradient-echo techniques such as MRDTI, T1-weighted TSE). Recent advances in susceptibility-weighted imaging may help to overcome this limitation by enabling the discrimination of calcification and IPH based on differences in susceptibility on filtered-phase images.[28] False-positive results, as we have seen, can result from the misidentification of perivascular adipose tissue for IPH. This limitation can often be addressed by using the arterial phase CE-MRA image to verify the lumen boundary and confirm the location of the hyperintensity within the wall on the coregistered mask image. 3) All MRA sequences

were acquired by using dedicated carotid coils, which are not widely used in routine evaluations for carotid stenosis. However, we have also observed hyperintense signal intensity corresponding with histologically confirmed IPH presence, even when using the body coil during routine clinical MRA evaluations for carotid stenosis in 2 patients, and IPH detection was also reported by Wintermark et al[18] in 3 patients by using a standard coil.

Conclusions

The CE-MRA mask images can detect IPH with excellent reliability and accuracy at 3T, without requiring additional imaging time beyond that needed to measure stenosis. Radiologists should include the identification of IPH in their routine evaluation of these images because it can provide important insight into plaque vulnerability and stroke risk beyond luminal narrowing measurements for which these images are generally acquired.

References

1. Raghavan P, Mukherjee S, Gaughen J, et al. **Magnetic resonance angiography of the extracranial carotid system.** *Top Magn Reson Imaging* 2008;19:241–49
2. **Beneficial effect of carotid endarterectomy in symptomatic patients with high-grade carotid stenosis: North American Symptomatic Carotid Endarterectomy Trial Collaborators.** *N Engl J Med* 1991;325:445–53
3. **Endarterectomy for moderate symptomatic carotid stenosis: interim results from the MRC European Carotid Surgery Trial.** *Lancet* 1996;347:1591–93
4. Chu B, Kampschulte A, Ferguson MS, et al. **Hemorrhage in the atherosclerotic carotid plaque: a high-resolution MRI study.** *Stroke* 2004;35:1079–84. Epub 2004 Apr 1
5. Takaya N, Yuan C, Chu B, et al. **Presence of intraplaque hemorrhage stimulates progression of carotid atherosclerotic plaques: a high-resolution magnetic resonance imaging study.** *Circulation* 2005;111:2768–75
6. Altaf N, Daniels L, Morgan PS, et al. **Detection of intraplaque hemorrhage by magnetic resonance imaging in symptomatic patients with mild to moderate carotid stenosis predicts recurrent neurological events.** *J Vasc Surg* 2008;47:337–42
7. Altaf N, Beech A, Goode SD, et al. **Carotid intraplaque hemorrhage detected by magnetic resonance imaging predicts embolization during carotid endarterectomy.** *J Vasc Surg* 2007;46:31–36
8. Singh N, Moody AR, Gladstone DJ, et al. **Moderate carotid artery stenosis: MR imaging-depicted intraplaque hemorrhage predicts risk of cerebrovascular ischemic events in asymptomatic men.** *Radiology* 2009;252:502–08
9. Takaya N, Yuan C, Chu B, et al. **Association between carotid plaque characteristics and subsequent ischemic cerebrovascular events: a prospective assessment with MRI—initial results.** *Stroke* 2006;37:818–23
10. Shinnar M, Fallon JT, Wehrli S, et al. **The diagnostic accuracy of ex vivo MRI for human atherosclerotic plaque characterization.** *Arterioscler Thromb Vasc Biol* 1999;19:2756–61
11. Fayad ZA. **MR imaging for the noninvasive assessment of atherothrombotic plaques.** *Magn Reson Imaging Clin N Am* 2003;11:101–13
12. Yuan C, Mitsumori LM, Ferguson MS, et al. **In vivo accuracy of multispectral magnetic resonance imaging for identifying lipid-rich necrotic cores and intraplaque hemorrhage in advanced human carotid plaques.** *Circulation* 2001;104:2051–56
13. Moody AR, Murphy RE, Morgan PS, et al. **Characterization of complicated carotid plaque with magnetic resonance direct thrombus imaging in patients with cerebral ischemia.** *Circulation* 2003;107:3047–52
14. Bradley WG Jr. **MR appearance of hemorrhage in the brain.** *Radiology* 1993;189:15–26
15. Yim YJ, Choe YH, Ko Y, et al. **High signal intensity halo around the carotid artery on maximum intensity projection images of time-of-flight MR angiography: a new sign for intraplaque hemorrhage.** *J Magn Reson Imaging* 2008;27:1341–46
16. Habibi R, Lell MM, Steiner R, et al. **High-resolution 3T MR angiography of the carotid arteries: comparison of manual and semiautomated quantification of stenosis.** *AJNR Am J Neuroradiol* 2009;30:46–52
17. Underhill HR, Yarnykh VL, Hatsukami TS, et al. **Carotid plaque morphology and composition: initial comparison between 1.5- and 3.0-T magnetic field strengths.** *Radiology* 2008;248:550–60
18. Wintermark M, Rapp JH, Tan J, et al. **Unmasking complicated atherosclerotic plaques on carotid magnetic resonance angiography: a report of three cases.** *J Vasc Surg* 2006;44:884–87
19. Balu N, Yarnykh VL, Scholnick J, et al. **Improvements in carotid plaque imaging using a new eight-element phased array coil at 3T.** *J Magn Reson Imaging* 2009;30:1209–14
20. Ekuni D, Firth JD, Putnins EE. **RNA integrity and in situ RT-PCR in dentoalveolar tissues after microwave accelerated demineralisation.** *Arch Oral Biol* 2006;51:164–69. Epub 2005 Aug 11
21. Bitar R, Moody AR, Leung G, et al. **In vivo 3D high-spatial-resolution MR imaging of intraplaque hemorrhage.** *Radiology* 2008;249:259–67
22. Kerwin WS, Liu F, Yarnykh V, et al. **Signal features of the atherosclerotic plaque at 3.0 Tesla versus 1.5 Tesla: impact on automatic classification.** *J Magn Reson Imaging* 2008;28:987–95
23. Fleiss J. *Statistical Methods for Rates and Proportions.* 2nd ed. New York: John Wiley & Sons; 1981:218
24. Cappendijk VC, Cleutjens KB, Heeneman S, et al. **In vivo detection of hemorrhage in human atherosclerotic plaques with magnetic resonance imaging.** *J Magn Reson Imaging* 2004;20:105–10
25. Ota H, Yarnykh VL, Ferguson MS, et al. **Carotid intraplaque hemorrhage imaging at 3.0-T MR imaging: comparison of the diagnostic performance of three T1-weighted sequences.** *Radiology* 2010;254:551–63
26. Joakimsen O, Bonaa KH, Stensland-Bugge E. **Reproducibility of ultrasound assessment of carotid plaque occurrence, thickness, and morphology: the Tromso Study.** *Stroke* 1997;28:2201–07
27. U-King-Im JM, Fox AJ, Aviv RI, et al. **Characterization of carotid plaque hemorrhage: a CT angiography and MR intraplaque hemorrhage study.** *Stroke* 2010;41:1623–29
28. Barnes SR, Haacke EM. **Susceptibility-weighted imaging: clinical angiographic applications.** *Magn Reson Imaging Clin N Am* 2009;17:47–61